NIRS-M-129

HIMAC-021

Relationship between CT number and Electron Density, Scatter Angle and Nuclear Reaction for Hadrontherapy Treatment Planning

Naruhiro MATSUFUJI, Hiromi TOMURA, Yasuyuki FUTAMI,

Haruo YAMASHITA, Akio HIGASHI, Shinichi MINOHARA,

Masahiro ENDO and Tatsuaki KANAI

(to be published in *Physics in Medicine and Biology*, **43**, 1-15 (1998))

October 1998

National Institute of Radiological Sciences

9-1, Anagawa-4, Inage-ku, Chiba-shi 263-8555 JAPAN

Relationship between CT number and Electron Density, Scatter Angle and Nuclear Reaction for Hadrontherapy Treatment Planning

Naruhiro MATSUFUJI †, Hiromi TOMURA †, Yasuyuki FUTAMI †, Haruo YAMASHITA †, Akio HIGASHI ‡, Shinichi MINOHARA §, Masahiro ENDO § and Tatsuaki KANAI †

† *Division of Accelerator Physics and Engineering, National Institute of Radiological Sciences, 4-9-1 Anagawa, Inage-Ku, Chiba, Chiba 263-8555 Japan*

§ *Medical Physics and Engineering Office, National Institute of Radiological Sciences, 4-9-1 Anagawa, Inage-Ku, Chiba, Chiba 263-8555 Japan*

‡ *Public Health Department, Hyogo Prefectural Government, 5-10-1 Shimoyamatedori, Chuo-Ku, Kobe, Hyogo 650-8567 Japan*

To be published in *Physics in Medicine and Biology (U. K.)* **43** (1998) 1-15.

submitted on December 15, 1997

1st revision: submitted on July 31, 1998

final revision: submitted on August 18, 1998

Contents

Abstract

The precise conversion of CT numbers to their electron densities is essential in treatment planning for hadrontherapy. Although some conversion methods have already been proposed, it is hard to check the conversion accuracy during practical therapy. We have estimated the CT numbers of real tissues by a calculational method established by Mustafa and Jackson. The relationship between the CT numbers and the electron densities was investigated for various body tissues as well as some tissue-equivalent materials used for a conversion to check the accuracy of the current conversion methods. The result indicates a slight disagreement at the high-CT number region.

A precise estimation of the multiple scattering, nuclear reaction and range straggling of incident particles has been considered as being important to realize higher level conformal therapy in the future. The relationship between these parameters and the CT numbers was also investigated for tissues and water. The result shows that it is sufficiently practical to replace these parameters for real tissues with those for water by adjusting the density.

1. Introduction

A highly energetic hadron beam, such as a beam of protons or carbon ions, has many desirable characteristics for radiotherapy. Particularly important characteristics from a physical point of view are the unique depth-dose distribution known as the 'Bragg curve', and less scattering in matter. These features lead to a much more localized irradiation dose to the tumor region than by using the conventional photon or neutron beams. The advantage enables us to treat even a tumor that is growing close to critical organs. We have carried out clinical trials at HIMAC (Heavy Ion Medical Accelerator in Chiba) using carbon beams since 1994.

To take the greatest advantage of this situation, it is necessary to try to minimize any unwanted dose exposure to healthy tissue at the stage of treatment planning. For this purpose, the tumor region as well as the critical organs should be precisely identified on tomographic images of the patient's body.

Using an X-ray CT scanner is a convenient and widespread method to obtain tomographic images. A not-overlookable problem of applying X-ray CT images to hadrontherapy treatment planning is the difference in the interaction process between using photons and hadrons. The degree of the reaction of hadrons with matter is well indexed by the stopping power (~electron density) of matter. It is therefore necessary to obtain the distribution of the electron density in the patient's body for treatment planning. Images taken with X-ray CT, however, denote the distribution of the photon's linear-attenuation coefficients in matter, shown as the CT number. The linear-attenuation coefficient is intrinsically inapplicable to give a direct description of the hadron's reaction. The difference causes a significant importance of conversion from the CT number to the stopping power with good precision.

For this purpose, some conversion ideas have been proposed. Chen *et al.* (1979) of LBNL, where the first pioneering effort of heavy-ion therapy was carried out (Tobias *et al.*, 1973), proposed the first conversion method. In their method, a one-to-one linear relationship is assumed between the CT numbers and the electron densities in some tissue-equivalent materials. The CT numbers of the materials are obtained by scanning them with an X-ray CT scanner used for daily treatment planning. On the other hand, the electron densities are deduced by measuring the relative water-equivalent range in the materials with a hadron beam.

The method was adopted by LBNL, and has been used by many other hadron-therapy facilities, such as MGH and HIMAC, Tsukuba (Japan). The method is now regarded as a *de facto* standard one.

Verifying the accuracy of the conversion process is important for quality assurance of the therapy. However, direct verification is quite difficult because there are no reliable methods for comparing the calculated dose distribution with the dose

distributed inside a real patient's body. Mustafa and Jackson (1983) developed a calculation method to estimate the CT number of a material. This method is useful for our study - such as investigating the accuracy of the conversion process and the extent of error.

A recent increase in medical demand for hadron therapy for treating a minute tumor or a tumor located near close to a highly sensitive critical organ makes it indispensable to refine the calculation model for ongoing treatment planning. It is thus inevitable to describe the physical behavior of hadrons in a body with good precision. Multiple scattering, the extent of nuclear reactions and range straggling are considered to be primary parameters from this point of view. Common treatment planning handles a patient's body as a mixture of water with various local densities. When considering the installation of these parameters for future treatment planning, it becomes useful to calculate these physical parameters both in real tissues as well as in water, and to estimate the error in between.

In this study, the CT numbers of many real-body tissues and some tissue-equivalent materials are deduced by following Mustafa and Jackson's method. The accuracy of the LBNL conversion method is then checked using the CT numbers together with that of a new one developed by the PSI group. Relationships between CT number and the physical parameters are investigated for body tissues and water to check whether water can be used as a substitution for a real body when simulating these parameters.

2. Method

The CT number of a material is derived by the calculation method proposed by Mustafa and Jackson (1983), instead of making a practical measurement with a CT scanner.

2.1. CT number of real tissues

The CT number of material i, H_i in Hounsfield units, was originally defined by Kouris *et al.* (1982) as

$$H_i = 1000 \frac{\mu_{M\,i} - \mu_{c\,i}}{\mu_{c\,i}} \quad . \tag{1}$$

Here, μ_{Mi} and μ_{Ci} are the linear-attenuation coefficient of the target material and the standard material (water), respectively, μ_{Mi} is expressed regarding the photon's energy spectra $\Omega(E)$ as follows:

$$\mu_{M\,i} = \frac{\int \Omega(E)\,\mu_M(E)\,dE}{\int \Omega(E)\,dE} \quad . \tag{2}$$

Hence, the CT number can be calculated by knowing two parameters, such as the energy spectra of X-ray CT ($\Omega(E)$) and the linear-attenuation coefficient of the material as a function of the energy (μ_M (E)). The linear-attenuation coefficients of real tissues were derived from the data of ICRU 46 (1992). There are 106 real tissues in the data table. The mass-absorption coefficient, chemical composition and electron density are given for each tissue. The tissues appearing in ICRU 46 are summarized in table 1.

The linear-attenuation coefficients of a compound ($\mu_{compound}$) that does not appear in ICRU46 was calculated by the following equation where ω_i , μ_i, ρ_i and $\rho_{compound}$ are the fraction by weight, linear-attenuation coefficient and density of element i, and density of the compound, respectively:

$$\mu_{compound} / \rho_{compound} = \sum_i \omega_i \mu_i / \rho_i \quad . \tag{3}$$

The linear-attenuation coefficient of each element was taken from data of Hubbell and Seltzer (1996).

The energy spectra ($\Omega(E)$) can be written in terms of the energy spectra at the source (S(E)) and the response function of the detector (D(E)) as

$$\Omega(E) = S_k(E) D(E) \exp\{-\int \mu_c(E)\,dx\} \quad . \tag{4}$$

Since the response of the detector (D(E)) is principally independent of the kind of target material, it can be considered as a constant in this study. The exponential term represents the attenuation effect of a photon along its path. It can also be regarded as being a constant, because the size or position of the target materials can be generalized in our study. For this reason, the energy spectrum of a typical X-ray CT is applicable as Ω(E) in this formalism. Fig. 1 shows the energy spectrum X-ray CT used in the calculation. The spectrum was measured by Matsumoto (1996) for primary X-rays from a HITACHI high-speed helical CT (LSCT) using a CdZnTe detector at the center of the CT gantry in free air. The voltage and current supplied to the X-ray tube was 120 kVp and 3 mA (6 s), respectively. An additional copper filter of 0.1 mm in thickness was inserted.

For all practical purposes, there are many additional factors that affect the actual CT number and cause uncertainties. A volume effect due to beam hardening, a field effect and the X-ray's energy spectra are usually taken into consideration as the principal physical factors. There are also some other problems: the intrinsic characteristic of the CT scanner due to a difference in its type or the manufacturer, a difference in the reconstruction algorithm, the way to process the artifact and so on. It is important to mention that these factors are not all dependent on the kind of target material, but are dependent on the secondary surrounding environments. It is thus required to equalize these factors for the purpose of discussing the fundamental problems involved in the conversion process and investigating the relationship between the physical parameters and the CT numbers. Therefore, these additional factors are not taken into consideration concerning this CT-number calculation. Fig. 2 shows the comparison of the calculated CT numbers with the values of Mustafa and Jackson (1983) for several tissue-equivalent materials. It can be said that our simplified CT number calculation is practical enough for the aim of this study.

2.2. Conversion method

2.2.1. LBNL's method

The tissue-equivalent materials used in this method are listed in table 2. In our study, the CT numbers of these materials derived by X-ray CT used for daily-treatment planning are replaced with the calculated ones.

The electron densities practically deduced by range measurements are also replaced by calculated values based on the chemical composition. As a result, the conversion curve is obtained by fitting them with an appropriate function (a bilinear function is normally adopted). The deduced function is directly applied to the human body for treatment planning.

2.2.2. PSI's method

A new conversion method was recently proposed by the PSI group (Schneider *et al.* 1996, Schaffner and Pedroni 1998). In their method, the CT numbers of several tissue-equivalent materials are first measured by X-ray CT used at the daily treatment planning, just as in LBNL's method. The tissue-equivalent materials used in the method are summarized in Table 3.

Next, linear-attenuation coefficients reduced from the CT numbers using eq. (1) are fitted with three parameters (K^{ph}, K^{coh} and K^{KN}) by Rutherford's model (1976) :

$$\mu_M(k) = (\rho Ng)_M \{K^{ph}\tilde{Z}^{3.62} + K^{coh}\hat{Z}^{1.86} + K^{KN}\} \quad , \tag{5}$$

where

$$\tilde{Z} = \left[\sum \lambda_i Z_i^{3.62}\right]^{1/3.62} \quad , \tag{6}$$

$$\hat{Z} = \left[\sum \lambda_i Z_i^{1.86}\right]^{1/1.86} \quad , \text{ and} \tag{7}$$

$$\lambda_i = N_g^i / N_g \quad . \tag{8}$$

Z and $(\rho Ng)_M$ is the effective atomic number and the electron density of material M, respectively. Here, the practical CT numbers are replaced by the calculated CT numbers. The result of a least-squares fitting gives K^{ph}, K^{coh} and K^{KN} as 3.5737×10^{-9}, 1.4152×10^{-7} and 5.1496×10^{-3}, respectively. Then, the CT number of real tissue is deduced by these three fitting parameters together with the effective atomic number and the electron density of the tissue. The conversion curve is finally obtained by fitting the deduced CT numbers with the electron densities of several typical tissues by appropriate functions. We divide CT number into some region and apply a linear function to each CT number region by following the PSI's method.

Conversion lines of these 2 methods are compared with each other and with the group of real tissues, respectively.

2.3. Physical parameters

The relationships between the CT number and the physical parameters, such as the scatter angle, the mean-free path length and the range straggling, were investigated both in real tissues and in water. The density of water was imaginary, amd adjusted to share the same electron density with a tissue having a certain CT number. A

comparison was made for 160 MeV protons and a 290 MeV/nucleon carbon beam, which are typically used in hadrontherapy.

2.3.1. Scatter angle

The scatter-angle determines the divergence and displacement of the incident beam in a patient's body. It is indispensable to estimate this parameter with good precision, especially for 3-dimensional conformal therapy. The scatter angle is a function of the atomic number of both the incident and target material, as well as the energy of incident particle. The angle was well-modelled by Mustafa and Jackson (1981) by taking into account the energy loss using Molière's formula (1947). With $\beta = v/c$ and $p = hk/2\pi$, $\theta_{1/e}$, the angle at which the distribution falls to $1/e$ of its value at $\theta = 0$, is calculated as follows:

$$\theta_{1/e} = \chi_c \sqrt{1.007\, B - 1.33} \tag{9}$$

where

$$B = 1.153 + 2.583 \log\left(\chi_c / \chi_\alpha\right)^2 \tag{10}$$

and

$$\chi_c^2 = 4\pi e^4 z^2 \int_0^t dt' \sum_i \frac{N_i(t') Z_i^2}{(\rho v)^2} \quad . \tag{11}$$

Here, z, Z, χ_c and χ_α are the atomic number of the projectile, the atomic number of the target, the characteristic angle and the screening angle, respectively. We followed the definition of χ_α by Mustafa and Jackson (1981), shown as eq. (33) in the paper. The scatter angle after passing through 2 cm thickness of every tissue was calculated using these equations.

2.3.2. Mean-free path length with respect to a nuclear reaction

The total number of incident particles is attenuated by nuclear reactions when passing through a material. The loss of incident particles not only causes the loss of the dose to be given by the primary particles on one side, but also causes secondary exposure by fragment particles on the other. It is required to grasp the extent of the reaction in order to control the dose distribution deposited inside a body.

The mean-free path length is applicable as an index of the reaction. The path length is considered to be a function of the incident energy and the mass numbers of the incident and target particles. An estimation of the path length is given by the cross-

section model used in a fragment reaction simulation code, 'hibrac' (Sihver *et al.*, 1995). In this code, the macroscopic reaction cross section (Σ_{react}) is expressed in eq. (12), where A_p and $A_{t,i}$ are the mass number of the projectile and the target nucleus (i), respectively:

$$\Sigma_{react} = \sum_i \left(N_i \sigma_{react,i} \right) \quad . \tag{12}$$

Here,

$$\sigma_{react,i} = \pi r_0^2 \left[A_p^{1/3} + A_{t,i}^{1/3} - b_0 \left(A_p^{-1/3} + A_{t,i}^{-1/3} \right) \right]^2 \tag{13}$$

$$b_0 = 1.581 - 0.876 \left(A_p^{-1/3} + A_t^{-1/3} \right) \quad . \tag{14}$$

N_i and r_0 are the number of elements (i) per unit volume and the constant of proportionality in the expression for the geometrical nuclear radius, $r_i = r_0 A_i^{1/3}$, respectively.

The mean-free path length (L_{react}) is given as the inversion of Σ_{react}. The loss of incident particles can be estimated by using L_{react}, as

$$I = I_0 \exp(-t / L_{react}) \quad . \tag{15}$$

Here, I_0, I and t are the number of incident particles at the origin and after passing through the material, and the thickness of the material, respectively.

2.3.3. Range straggling

The total number of collisions and / or the energy loss per collision has some statistical fluctuation. Therefore, most of physical parameters used in treatment planning, such as the specific energy loss, energy, range and so on, are all an average of the fluctuating values. The extent of the fluctuation becomes important when estimating the dose distribution near to some critical tissue. From this point of view, the range straggling was calculated.

According to Payne's calculation (1969), the range straggling ($<\Delta R>^2$) is given by

$$< \Delta R >^2 = 4\pi Z_p^2 e^4 n A_p \int_E^{E_0} \frac{1-\beta^2/2}{(1-\beta^2)(1+\frac{2m_e}{M_p}\gamma)} \frac{K dE'}{[f(E')]^3} \quad . \tag{16}$$

Here, Z_p, A_p and M_p are the atomic number, mass number and mass of the projecticle, respectively, K is known as the low-energy correction term of Sternheimer (1960).

3. Results and Discussion

3.1. Variation of the CT number

Fig. 3 shows the relationship between the CT numbers and electron densities of real tissues. The cross symbols represent real tissues of ICRU 46. Most of the soft tissues gather in this area in a crowd. The line in fig. 4 indicates the result of a linear least-squares fitting to these soft tissues. From the result, the standard deviation (σ) of the electron density relative to water was deduced by calculating the distance between the fitting line and the data for the tissues. σ was derived as 0.0082. This indicates that the electron density of each CT pixel at around a CT number of 0 may vary by $\pm$ 0.82 % in σ.

There are two ways to consider the influence of the deviation to the total range of the variation. The first is the case that adjacent CT pixels have no correlation with each other. In this case, the variation in the electron density in each pixel can be regarded as being independent phenomena, therefore, the total range variation is statistically reduced by the square-root of the number of CT pixels. When considering the size of one CT pixel as 1 mm and range of the incident beam as 200 mm, the final variation of the range in this case is estimated as:

$$\frac{200\ mm \times \pm 0.82\ \%}{\sqrt{200}} \cong \pm 0.116\ mm \quad . \tag{17}$$

The second is the case that every pixel completely correlates to the adjacent pixels. In this case, a statistical reduction of the deviation can not be expected, and the variation directly results in a variation of the range. In this case, the final range variation is expected to be

$$200\ mm \times \pm 0.82\ \% \cong \pm 1.64\ mm \quad . \tag{18}$$

It is known that the practical CT number, itself, can vary by less than 1 percent, even for a uniform target, because of an intrinsic uncertainty of the measurement. The practical case is considered to be in between. The extent of the variation discussed here can be comparable with the intrinsic uncertainty. In the case of our typical treatment planning, we add 5 mm of margin around the target region. All of the considerable error caused by dosimetry, treatment planning, patient positioning, the movement of organ, and so on, are expected to be absorbed in the margin. The error from this variation should also be involved. Therefore, in the case that other error factors may account for the greater part of the margin, for example, with the irradiating beam through a highly complicated bone structure (the dosimetry error

will be larger) or the reference point for patient positioning is obscure (positioning error will be larger), an extra margin that can compensate for the error due to the variation is needed.

3.2. Appropriateness of conversion methods

The conversion lines derived from both methods are shown in fig.5. The solid line corresponds to LBNL's conversion curve. The line comprises the relationship due to ethyl alcohol below a CT number of 0, and by potassium phosphate over a CT number of 0. The modification is applied for use at our institute in order to show better agreement to real tissues, i.e., the line of ethyl alcohol is extended to a CT number of 50, and then jump to that of potassium phosphate. A PSI's conversion line is shown as the dotted one.

As a result, LBNL's conversion line shows good agreement with real tissues in the low and medium CT number area (lung to many soft tissues). However, a difference appears at the high-CT number area (bone). On the other hand, PSI's conversion line retains good agreement over the entire range. The difference between both methods reaches a maximum of 2.6 % in the high-CT number region.

The main reason that causes this difference is considered to be the difference in the characteristics of the reaction with hadrons between tissue-equivalent materials and real body tissues. These tissue-equivalent materials were originally developed to have equivalency with real tissues for photons, not hadrons. Therefore, their reaction characteristics are not always equivalent to those of real tissues. The newly developed PSI method also uses tissue-equivalent materials. However, the advantage of this method is that the use of tissue-equivalent materials is limited to describe the characteristics of the X-ray CT. This method is one of the effective ways to overcome the limitation that the current tissue-equivalent materials involve.

3.3. Scatter angle, mean-free path length and straggling

Figs. 6 and 7 show the scatter angle for 160 MeV protons and a 290 MeV/nucleon carbon beam, respectively. The cross symbols and the solid line represent the angles in real tissues on ICRU 46 and in water for various densities, respectively. At a high-CT number region, it is found that the scatter angle in water tends to underestimate that of real tissues. The difference between them becomes larger as the CT number becomes conspicuous, and reaches about 10% at a CT number of 1000. The angle, itself, is smaller in the case of carbon than proton, because of the heavier weight of the carbon nucleus, however, a difference also appears.

Figs. 8 and 9 show the mean-free path length with respect to nuclear reaction of

proton and carbon beams in tissues and water, respectively. The symbols are identically the same as in the case of the scatter angle. The difference between tissues and water shows the same tendency as in the case of the scatter angle. At a CT number of 1000, the mean-free path length is 62.3 cm in tissue, whereas it is 56.1 cm in water for a 160 MeV proton beam. The difference causes a 2% difference in the total fluence at the end of the range after passing through 2 cm of a high-CT material at the entrance and water in the residual.

As for range straggling, the results are summarized in figs. 10 and 11 for proton and carbon beams, respectively. From these results, it is found that range straggling in real tissues is well simulated with water within 0.1 mm of accuracy.

The case of a simulation using a proton beam was treated in order to judge if the differences in multiple scattering or a nuclear reaction cause any practical problems or not. The geometrical alignment for the simulation is as follows. The main frame is composed of uniform water (density of 1.00 g/cm^3) as a substitute for soft tissues. A high-CT number material (CT of 1000) of 20 mm in thickness is placed at the entrance region of water as a substitute for bone. A calculation was made for 2 cases: in the first one the high-CT number material was made of real bone, in the other one it was made of liquid water.

The displacement of the incident particle from the beam axis and the depth-dose distribution curve was calculated for the 2 cases. The displacement is related to the scatter angle. Eq. (9) was used for the calculation. The dose distribution is related to the nuclear reaction cross section and the electron density of the material. The energy loss in the material was calculated using a calculation code developed at LBNL (Salamon, 1980).

The results due to the difference in the dose distribution and the rate of deflection from the beam axis are shown in figs. 12 and 13, respectively. Dashed line in fig. 12 represents the difference of dose in % except the Bragg-peak point. As for the dose distribution, it produces no obvious variation at the entire pedestal region of depth-dose profile if the real bone is regarded as being liquid water. A slight difference in the deflection by about 0.1 mm at the vicinity of the beam range is found. However, the rate is small enough to be neglected.

4. Conclusion

The electron densities of real soft tissues have ±0.82% of standard deviation. If adjacent CT pixels have a complete correlation, the deviation causes ±0.82% of a range variation. It may be reasonable to consider that the adjacent CT pixels have a certain correlation. Therefore, it is necessary to take into consideration the ±0.82% range variation produced by the CT number variation for safety when setting the margin on treatment planning.

As for the conversion methods, the calibration curves from both the conventional LBNL method and the new PSI method trace well to the relationship of real tissues. However, LBNL's method produced about a 2.6% error in the high-CT number region. PSI's method is a simple, but useful, way to reduce the extent of the conversion error.

It is precise enough for practical treatment planning to simulate the scatter angle or the mean-free path length in real tissues with water. However, in the case where the greater part of the beam path is occupied by high-CT number materials, it is necessary to use some other material that has a similar composition to that of bone for simulating these physical parameters.

Acknowledgments

Authors wish to thank Dr. Masao Matsumoto of Osaka University for presenting us his significant data about the energy spectra of the X-ray CT. We are also thankful to all the staff at HIMAC for their kind support to this work.

4. Conclusion

The electron densities of real soft tissues have ±0.82% of standard deviation. If adjacent CT pixels have a complete correlation, the deviation causes ±0.82% of a range variation. It may be reasonable to consider that the adjacent CT pixels have a certain correlation. Therefore, it is necessary to take into consideration the ±0.82% range variation produced by the CT number variation for safety when setting the margin on treatment planning.

As for the conversion methods, the calibration curves from both the conventional LBNL method and the new PSI method trace well to the relationship of real tissues. However, LBNL's method produced about a 2.6% error in the high-CT number region. PSI's method is a simple, but useful, way to reduce the extent of the conversion error.

It is precise enough for practical treatment planning to simulate the scatter angle or the mean-free path length in real tissues with water. However, in the case where the greater part of the beam path is occupied by high-CT number materials, it is necessary to use some other material that has a similar composition to that of bone for simulating these physical parameters.

Acknowledgments

Authors wish to thank Dr. Masao Matsumoto of Osaka University for presenting us his significant data about the energy spectra of the X-ray CT. We are also thankful to all the staff at HIMAC for their kind support to this work.

References

Chen G T Y, Singh R P, Castro J R, Lyman J T and Quivey J M 1979 Treatment planning for heavy ion radiotherapy *Int. J. Radiation Oncology Biol. Phys.* **5** 1809-1819

Hubbell J H and Seltzer S M 1996 Tables of X-ray mass attenuation coefficients and mass energy-absorption coefficients 1 keV to 20 MeV for elements Z = 1 to 92 and 48 additional substances of dosimetric interest *NISTIR* **5632** *(Web version 1.02: http://physics.nist.gov/PhysRefData/XrayMassCoef/cover.html)*

ICRU 1992 Photon, electron proton and neutron interaction data for body tissues *ICRU Report* **46**

Kouris K, Spyrou N M and Jackson D F 1982 *Imaging with ionizing radiations* (Glasgow, Surrey University Press)

Molière G 1947 *Z. Naturforsch.* a **2** 133

Matsumoto M. 1996 *private communication.*

Mustafa A A M and Jackson D F 1981 Small-angle multiple scattering and spatial resolution in charged particle tomography *Phys. Med. Biol.* **26** 461-472

———— 1983 The relation between x-ray CT numbers and charged particle stopping powers and its significance for radiotherapy treatment planning *Phys. Med. Biol.* **28** 169-176

Payne M G 1969 Energy Straggling of Heavy Charged Particles in Thick Absorbers, *Phys. Rev.* **185** 611-623

Rutherford R A, Pullan B R and Isherwood I 1976 Measurement of effective atomic number and electron density using an EMI scanner Neuroradiology 11 15-21

Salamon M H 1980 A Range-Energy Program for Relativistic Heavy Ions in the Region 1<E<3000 MeV/amu *LBL Report* **10446**

Schaffner B and Pedroni E 1998 The precision of proton range calculations in proton radiotherapy treatment planning: Experimental verification of the relation between CT-HU and proton stopping power *Phys. Med. Biol. To be published*

Schneider U, Pedroni E and Lomax A 1996 The calibration of CT Hounsfield units for radiotherapy treatment planning *Phys. Med. Biol.* **41** 111-124

Sihver L, Tsao C H, Silberberg R, Barghouty A F and Kanai T 1995 Calculations of depth-dose distributions, cross sections and momentum loss *Adv. Space. Res.* **17** 105-108

Sternheimer R M 1960 Range straggling of charged particles in Be, C, Al, Al, Cu, Pb, and air *Phys. Rev.* **117** 485-488

Tobias C A, Wenke R P and Benton E V 1973 Heavy-particle radiotherapy *Nature* **182** 474-476

Table 1. List of real tissues of ICRU 46. Number in parentheses denotes the number of subdivision by age bracket.

Adipose tissue (13), Average soft tissue (3), Blood (3), Bone mineral, Brain (4), Breast (6), Carbohydrate, Cell nucleus, Eye lens, Gallstones, GI tract, Heart (6), Kidney (3), Lipid, Liver (5), Lung (3), Lymph, Muscle (4), Ovary, Pancreas, Placenta (2), Protein, Skeleton (30), Skin (3), Spleen (2), Testis, Thyroid, Urinary bladder (2), Urinary stones (3), Water. (106 in total)

Table 2. List of tissue-equivalent materials used in LBNL's conversion method.

tissue	substitution
bone	solution of K_2HPO_4 (0~40 % vol.)
fat and soft tissues	solution of C_2H_5OH (0~100 % vol.)
lung	lung phantom or cork

Table 3. List of tissue-equivalent materials used in PSI's conversion method.

tissue	substitution
fat	AP6
muscle	MS/SR4
soft bone	IB/SR1
skeleton	TSK/SR1
soft tissue	HB/SR4 and water

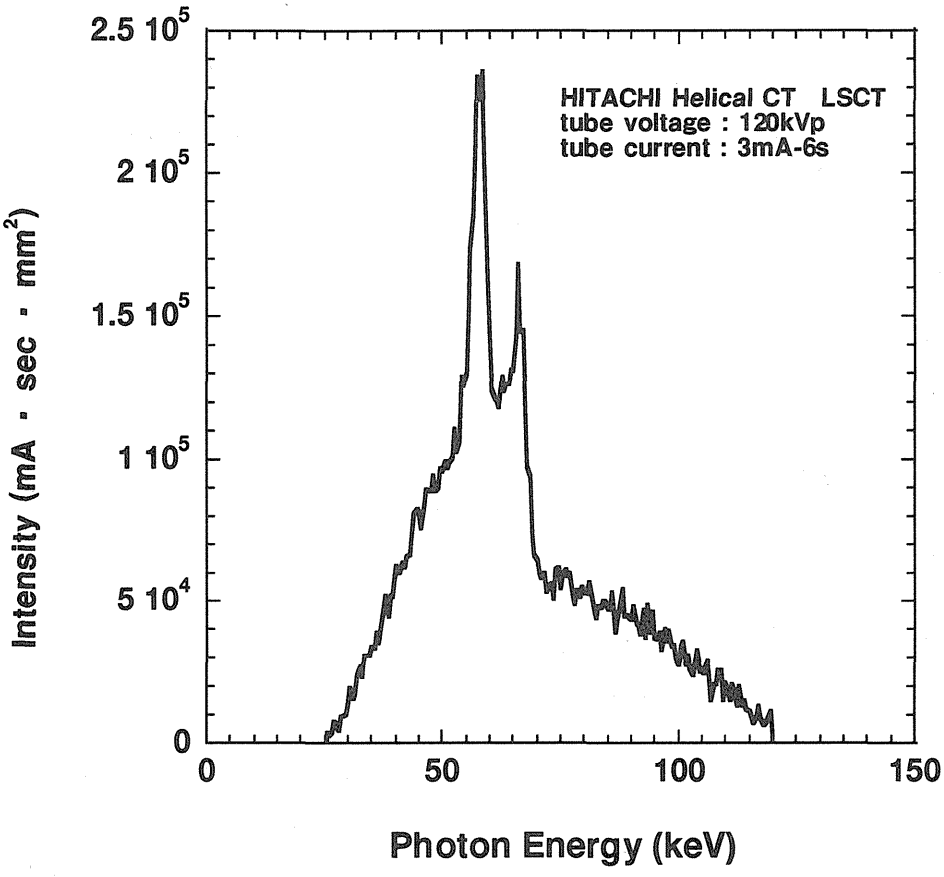

Fig. 1 Energy spectra of HITACHI LSCT. Voltage and current of tube is 120kVp and 3mA (6s), respectively.

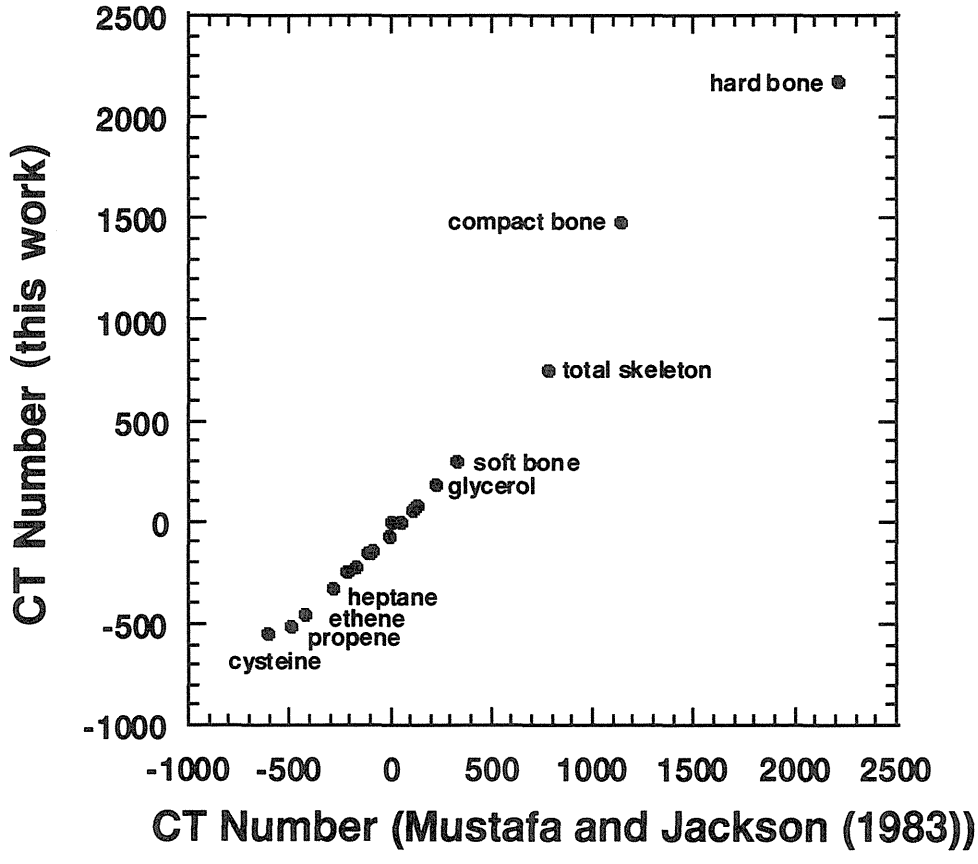

Fig.2 Comparison of CT number calculation with Mustafa and Jackson (1983) for several tissue-equivalent materials.

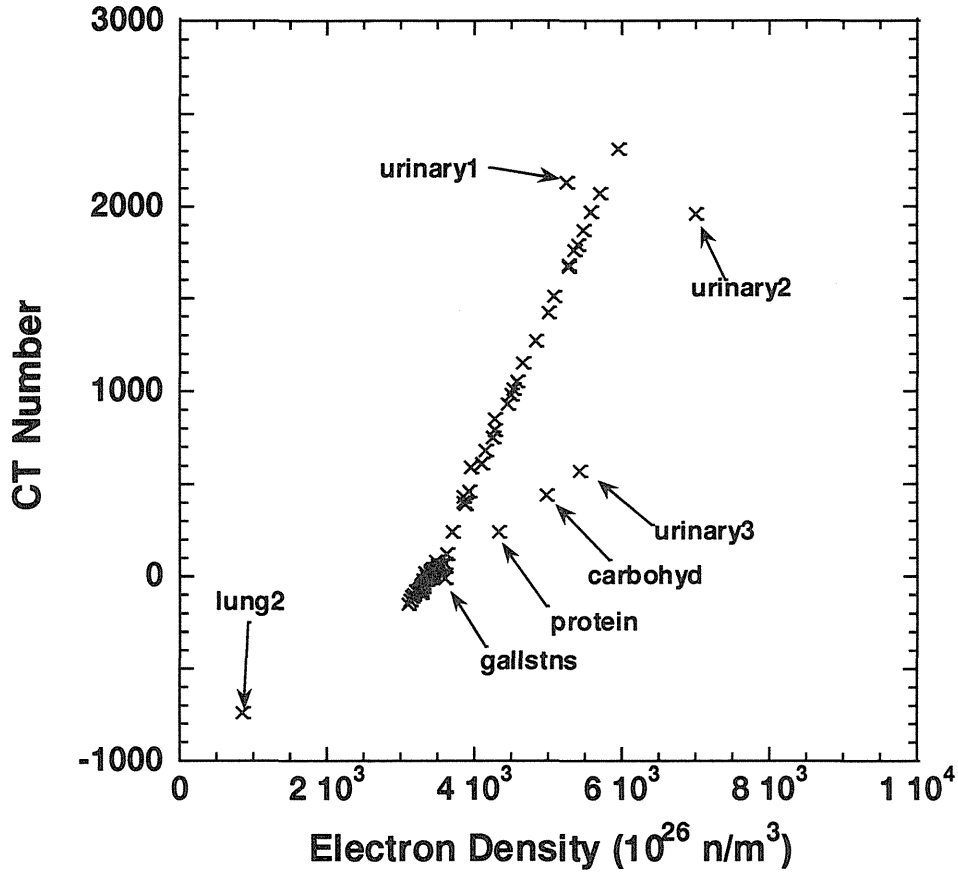

Fig.3 Relationship between electron density and CT number of real body tissues of ICRU46.

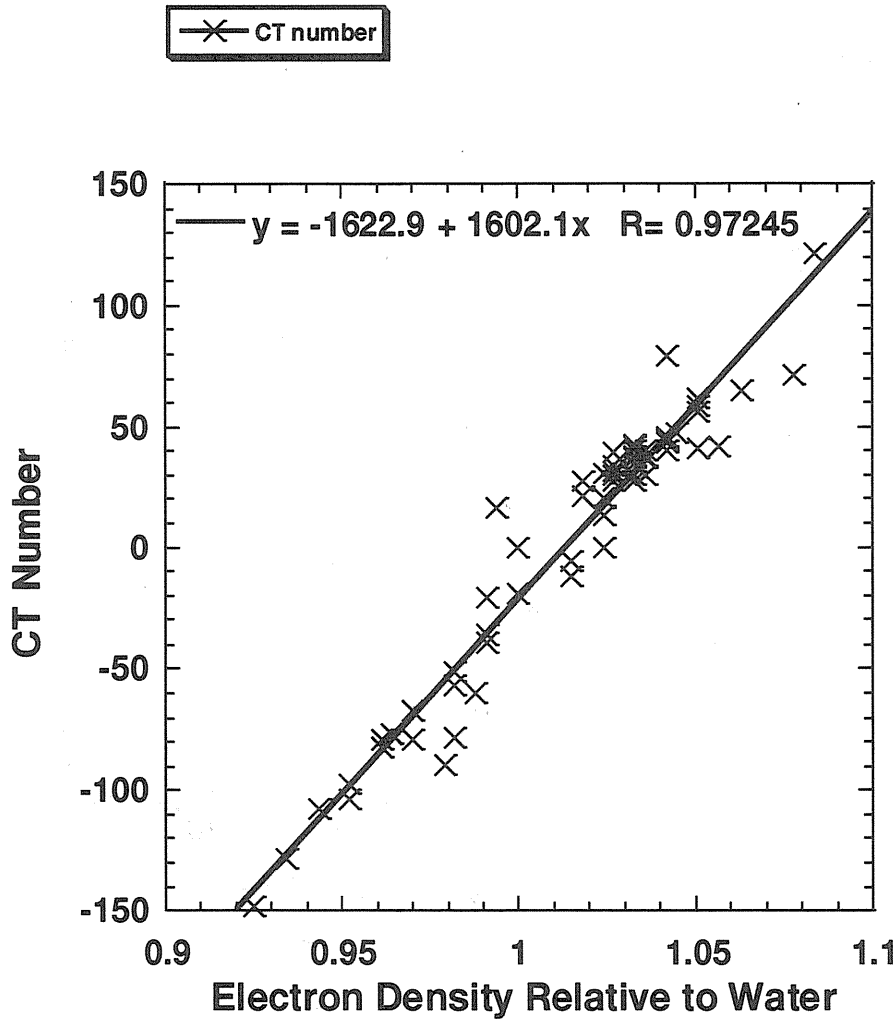

Fig.4 Relationship between electron density and CT number of real body tissues (magnified). Solid line represents the result of linear least square fitting.

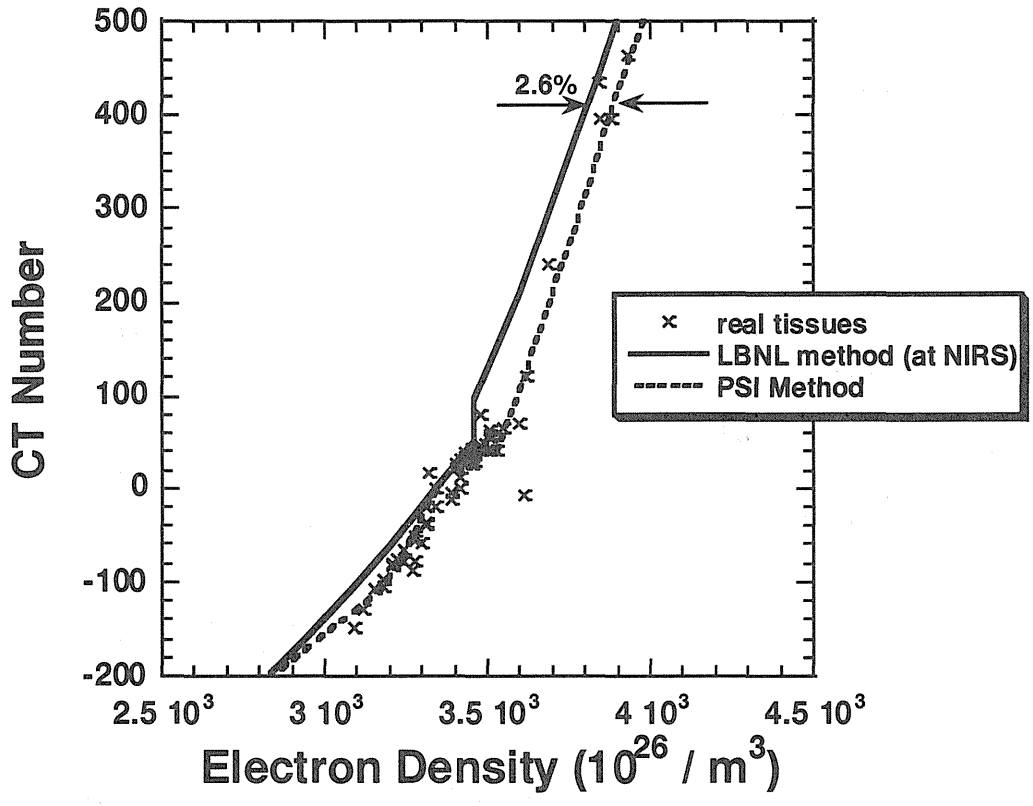

Fig.5 Relationship between LBNL and PSI conversion lines and real tissues.

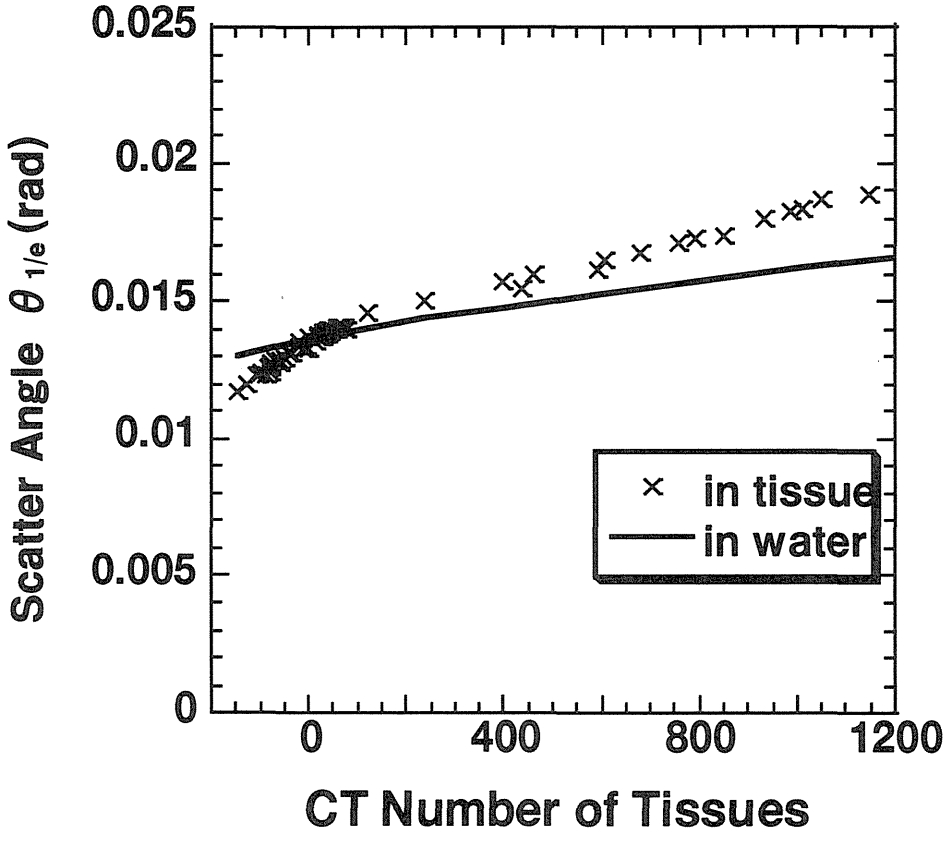

Fig.6 Scatter angle of proton in real tissues and water of 2 cm in thickness.

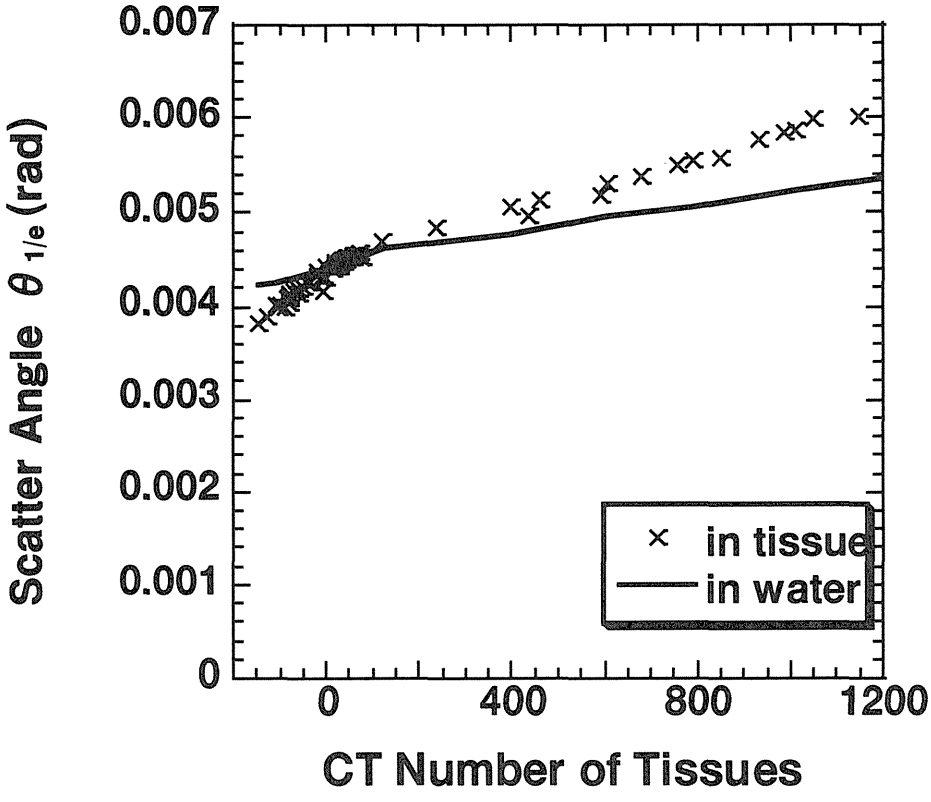

Fig.7 Scatter angle of carbon in real tissues and water of 2 cm in thickness.

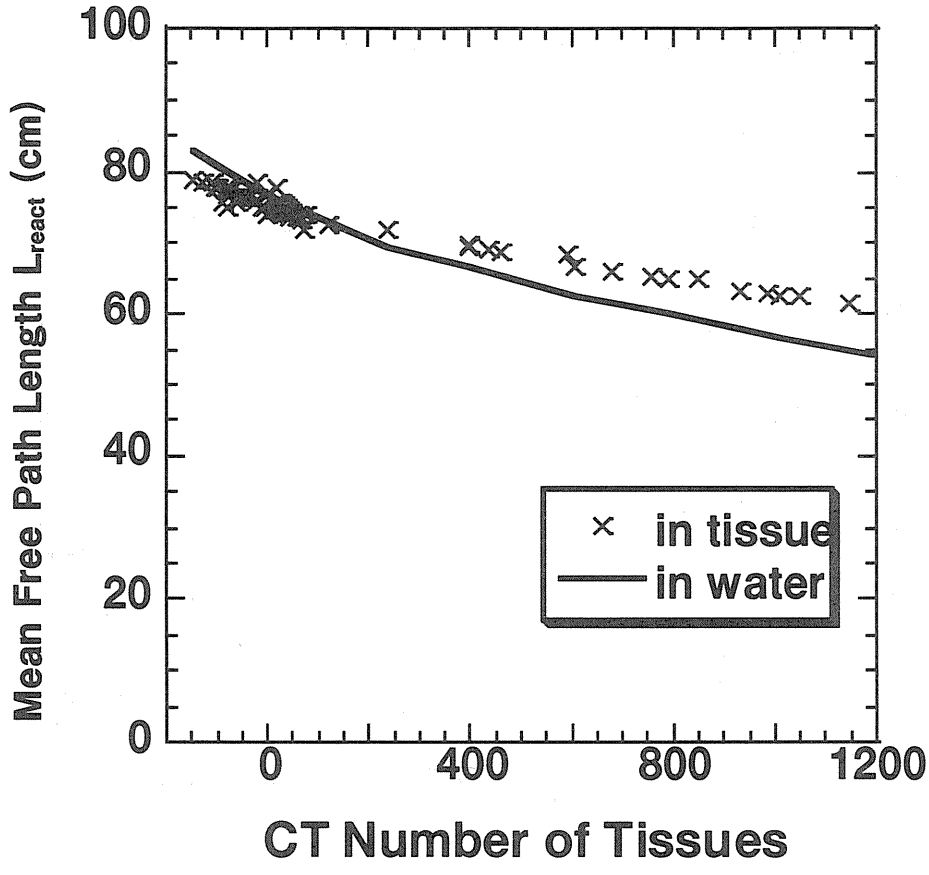

Fig.8 Mean-free path length of 160 MeV protons in real tissues and water.

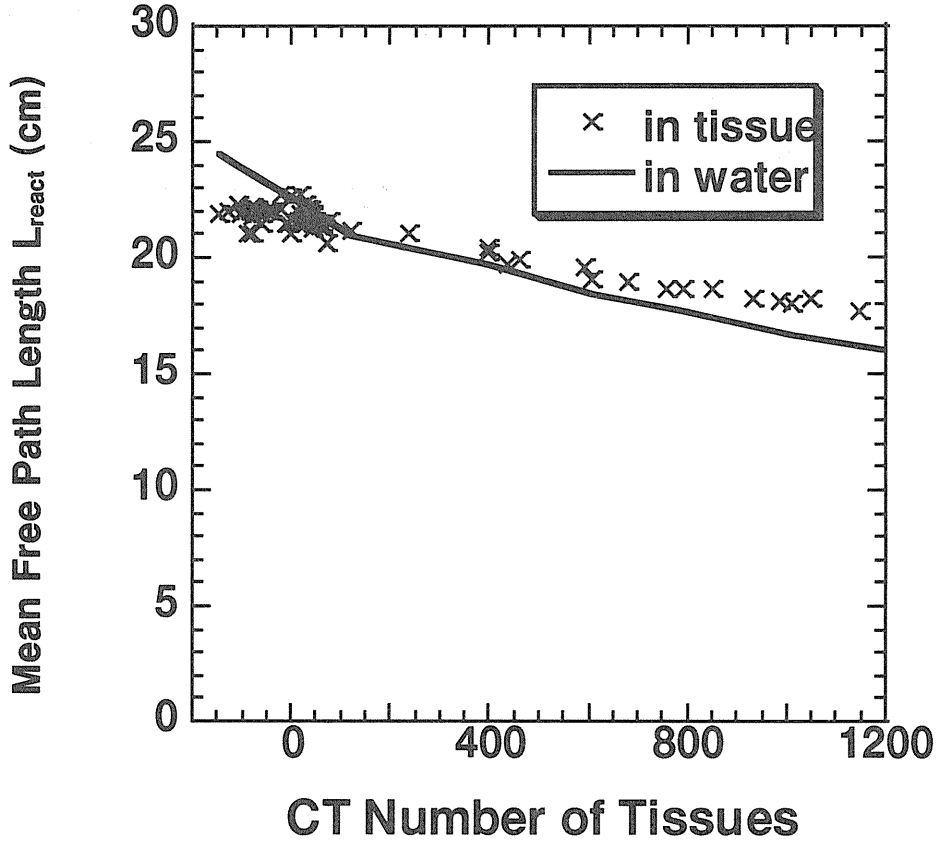

Fig.9 Mean-free path length of 290 MeV/nucleon carbon projectiles in real tissues and water.

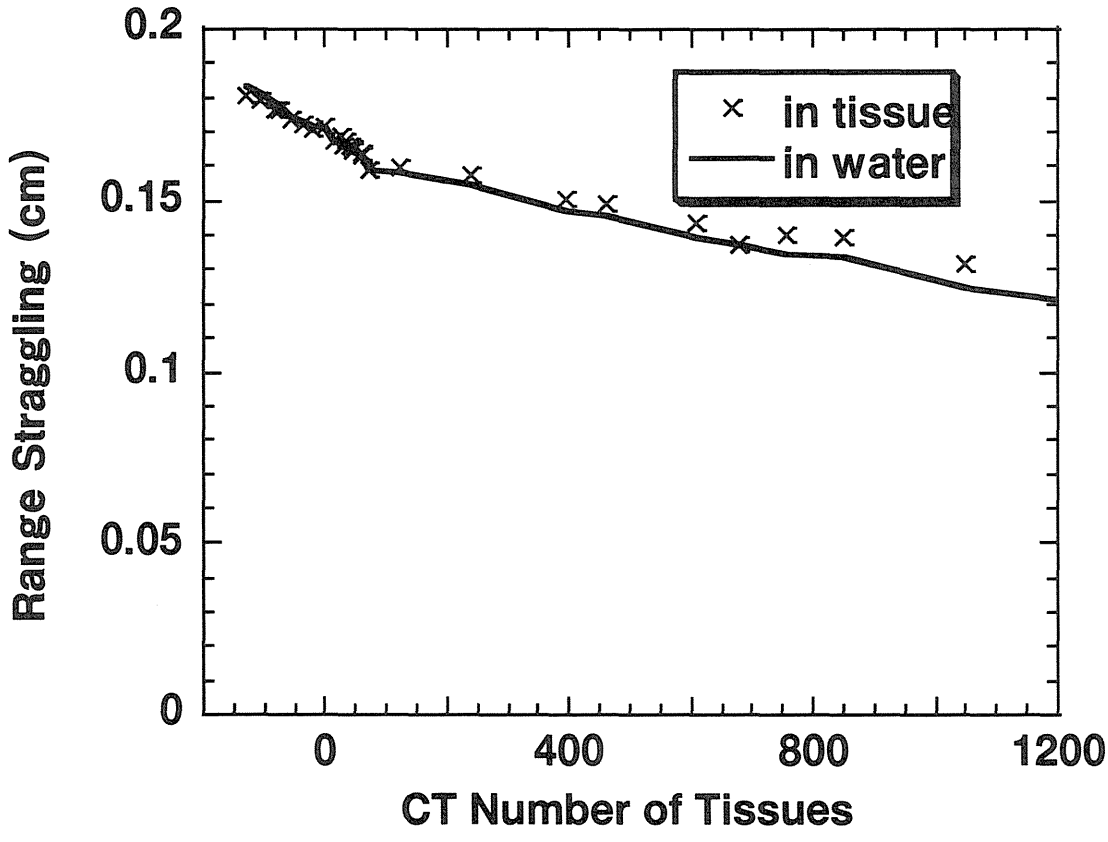

Fig.10 Range straggling at the range-end of 160 MeV protons.

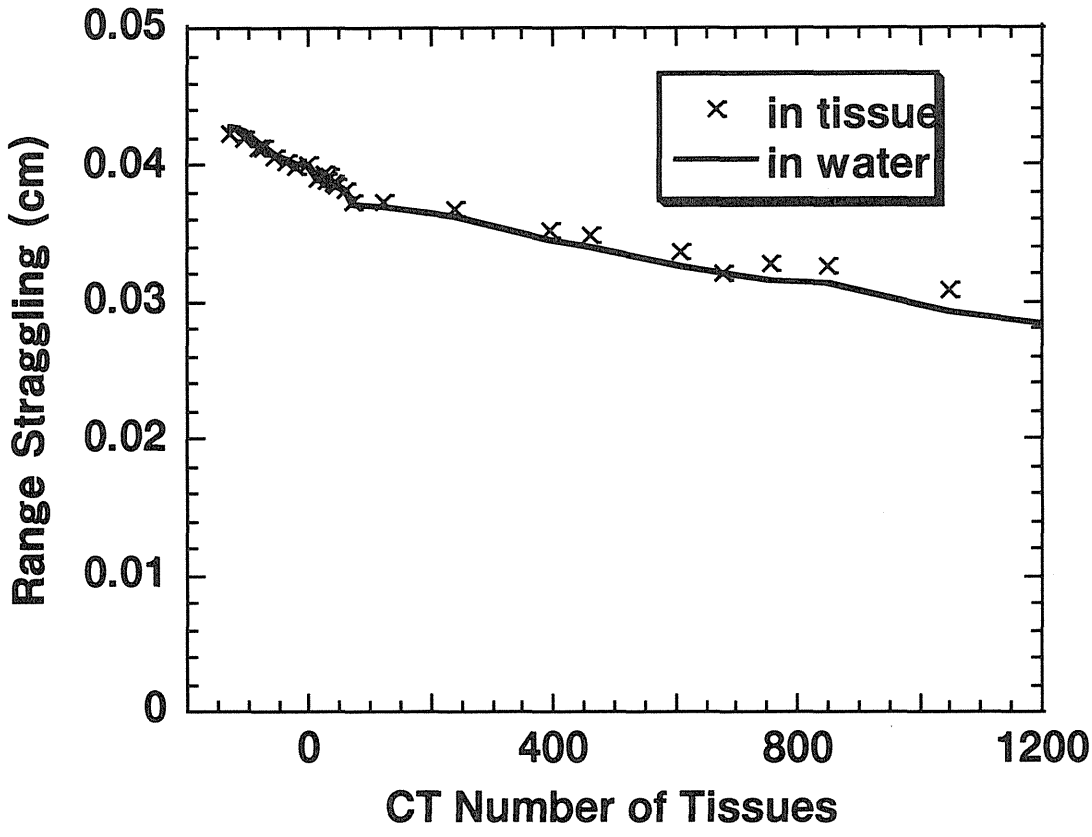

Fig.11 Range straggling at the range-end of 290 MeV/nucleon carbon projectiles.

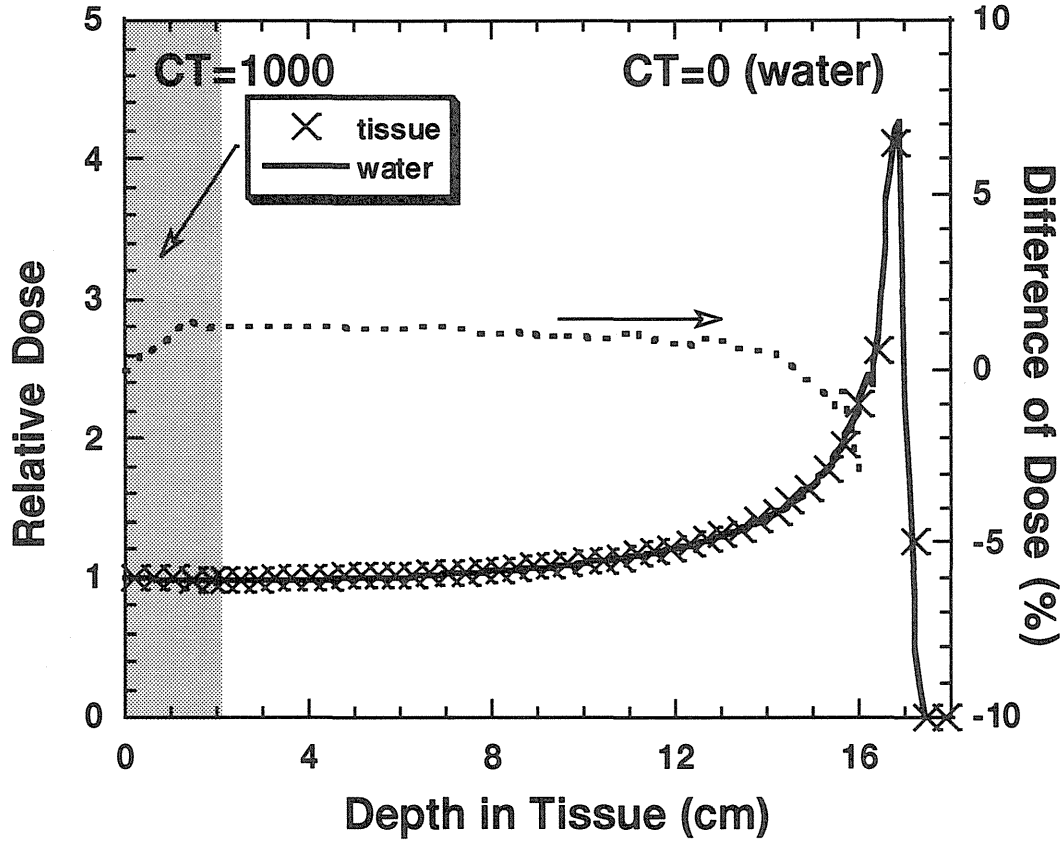

Fig.12 Depth dose distribution of 160 MeV of proton. A material, which has CT number of 1000, of 2cm in thickness is positioned at surface. Solid line and cross symbols correspond to the case that the material is made of liquid water and real bone, respectively. Dashed line represents the difference of dose between the cases.

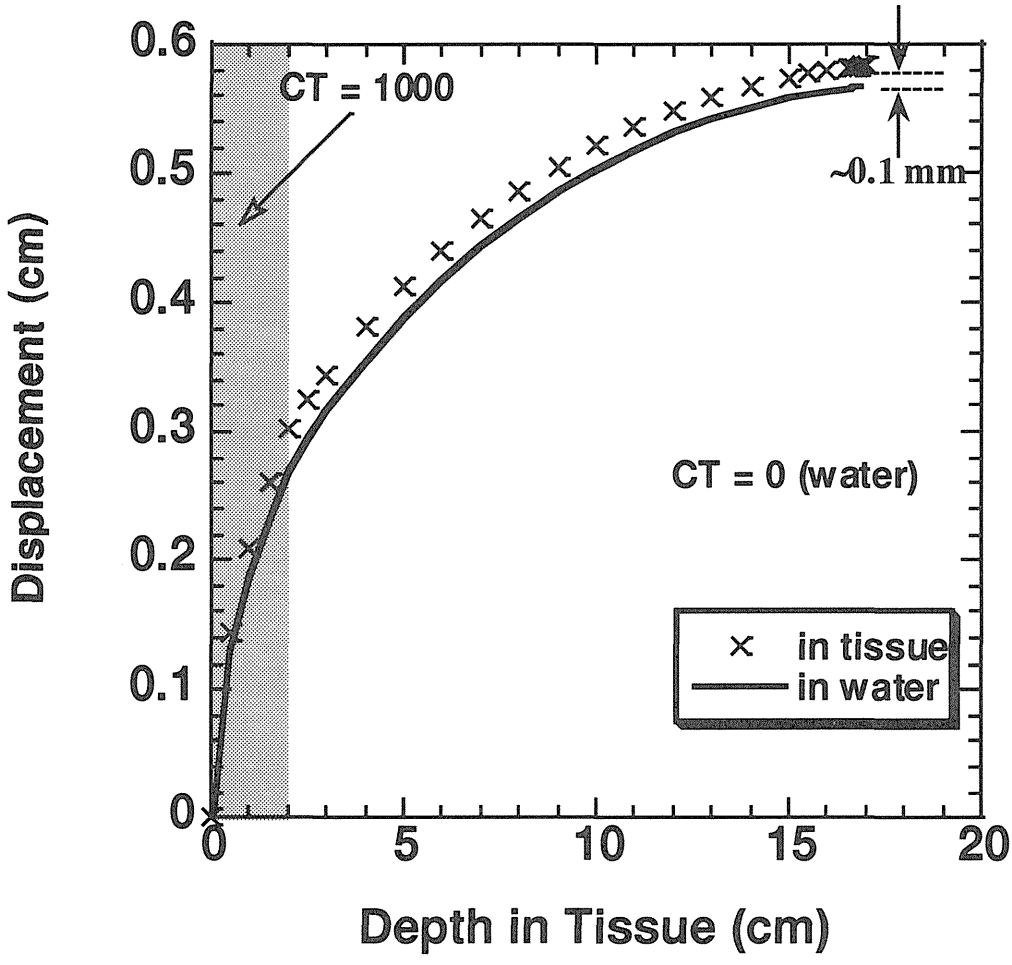

Fig.13 Displacement of 160 MeV proton beam from beam axis. The High CT number material is positioned at entrance. Solid lines and cross symbols are identical to those in fig.12.